

Determination of Young's Modulus of Metallic and Composite Materials by Digital Image Correlation

M. Zeeshan Siddiqui, Fawad Tariq, Nausheen Naz, M. Fahad Ahmed

Abstract—Accurate determination of Young's Modulus of materials is important for structural design, analyses, as well as for quality control. The intricacies involved in such experiments are generally related to the accurate measurement of strains in the elastic region. For metals and composite laminates, the problem is generally dealt with the use of extensometers or strain gages. In case of fiber tows, such simple solution is often restricted by the small specimen size and low bending rigidity of the specimen. This paper presents an alternative approach for the determination of in-plane Young's modulus of these materials by using Digital Image Correlation (DIC). Uniaxial tensile experiments were performed with specimens made of aluminum alloy, E-Glass/Polyester laminate and carbon fiber tows with strain measurement done through an indigenously developed two dimensional DIC algorithm in MatLab. The strain measurements were validated for aluminum alloy and composite specimens by using foil-type electric resistance strain gages. The elastic modulus computed with these strain values were then compared with literature data. The comparison shows good agreement with the reference values. The proposed technique offers a quick, cost-effective and widely adaptable alternative of traditional methods for determination of elastic modulus of both homogeneous as well as heterogeneous materials.

Index Terms—Composites, Digital Image Correlation, Optical Strain Measurement, Young's Modulus

I. INTRODUCTION

THE knowledge of elastic constant of materials is indispensable for structure design and quality control purposes. Thus its determination is of utmost importance to all engineering applications. The Young's modulus or modulus of elasticity E is the property which describes the deformation behavior of a material or structure under loading. Materials deform differently when loads are applied, and the relationship between stress and strain is typically defined by the Young's modulus. The ability of any material to resist or transmit load is important, and this property is often used to determine if a particular material is suitable for a specific purpose.

The value of elastic constants can be experimentally determined by different methods. Methods of determination are further classified into "Direct" and "Indirect" methods. In direct methods, these constants are determined from the longitudinal and transverse deformations as well as by the effects which depend directly on them; whereas, in the indirect methods these are determined from the measurement of other elastic constants like Shear or Bulk moduli. In static methods, these constants are determined by the deformations produced by the time dependent or slowly changing forces in contrast to dynamic methods which often involve vibration studies [1]. For general engineering applications static methods are widely utilized by engineers and scientist.

Mostly, the Young's modulus E is derived from the slope of the linear part of the stress-strain curve during uniaxial tensile testing. For getting accurate values of E , the strain data should be reasonably accurate which is generally obtained from either using foil strain gages or clip-on extensometers. However, the use of strain gages and extensometers is sometimes limited because of cost involved, and the size and shape of specimen under test. Beside this traditional technique, several other methods are documented in literature for accurate determination of Young's modulus (E) of materials. One is ultrasonic pulse-echo technique [1]-[3]. In this method, an ultrasonic beam is generated by a transducer which is attached to the measured materials. By measuring the sound velocity in the medium, the elastic properties can be determined. The other is the resonance method [4], [5]. By measuring the resonant frequency, elastic properties can be calculated because resonant frequency is related to the structure's geometry as well as the elastic properties. Indentation methods (micro and nano) are also widely adopted for determining young's modulus where value of E is determined directly from indentation load and displacement data obtained during one cycle of loading and unloading [6]-[11]. This method is very famous because relatively small amounts of testing materials are needed and there are no strict requirements for sample shape. Some authors have also successfully used non-destructive Eddy Current technique (combined a/c and d/c magnetic fields) to evaluate Young's modulus of solids [12], [13]. In the present paper, the direct measurement approach has been employed wherein the strain measurement has been done through Digital Image Correlation (DIC). From the outcome of this work it is expected that this technique will prove very useful for determination of Young's modulus, particularly in those cases where the use of strain gage or extensometer is not applicable.

II. PROCEDURE FOR MEASUREMENT OF YOUNG'S MODULUS

For a uniaxial tensile test, the Young's modulus (E) is defined as the ratio between stress and strain during the elastic region. For metallic specimens, it is given as:

$$E = \frac{P}{A \times \epsilon} \quad (1)$$

Where:

P is the load measured during the elastic region through a load cell;

A is the cross-sectional area of the specimen;

ϵ is the elastic strain;

For composite laminates, the quantity E is termed the chord modulus (Fig. 1) and is calculated as:

$$E = \frac{P_u - P_l}{A \times (\varepsilon_u - \varepsilon_l)} \quad (2)$$

Where:

- E is the chord modulus as defined in fig. 1
- P_u is the tensile load at upper strain limit;
- P_l is the tensile load at lower strain limit;
- ε_u is the upper strain limit;
- ε_l is the lower strain limit;

The cross sectional area A of fiber tows is calculated with the equation:

$$A = \frac{MUL}{\rho_f} \quad (3)$$

Where:

- MUL is the fiber mass per unit length
- ρ_f is the fiber bulk density

The strain ε appearing in (1) and (2) is the quantity of interest that has to be measured experimentally using a suitable strain measurement device. The strain measurement, in this work, has been done by extracting the surface strain values from displacement data acquired through simple experimental setup consisting of digital camera and numerical algorithm for Digital Image Correlation devised in MatLab. For comparison, the Young's modulus has also been determined by measuring strain from electric-resistance strain gages and extensometers.

III. DIGITAL IMAGE CORRELATION

When an object undergoes deformation, each point on the surface of the object moves in coherence with its neighborhood. This coherence introduces a similarity between the images of object surface before and after deformation. Digital Image Correlation (DIC) works by matching this similarity across images of the object surface taken before and after deformation. The images for correlation matching can be acquired either by using a simple tripod mounted digital camera or through a microscope (optical, SEM or TEM). Selection of image capturing device depends on the dimensions of the specimen or strain levels to be measured. As the object deforms, points in the initial or reference image (left image in Fig. 2) move to new positions in the deformed or target image (right image in Fig. 2). The correlation algorithm goes through a set of selected points in the reference image and finds their corresponding matches in the reference image based on the optimum value of matching criterion. Once the positions of all the points have been determined, smoothing is applied to remove noise, and strain computations may be carried out. The matching criteria for finding the best match can be least squares, absolute integral error or correlation coefficient. In this work, correlation coefficient is

computed by (4)

$$C = \frac{\sum_i \sum_j (R_{ij} - \bar{R})(T_{ij} - \bar{T})}{\sqrt{\sum_i \sum_j (R_{ij} - \bar{R})^2 \sum_i \sum_j (T_{ij} - \bar{T})^2}} \quad (4)$$

Where R_{ij} , T_{ij} are intensity values at each pixel for the reference and target images respectively while \bar{R} , \bar{T} are corresponding mean intensities of the entire images. The correlation surface near the optimum point, which is in the vicinity of target location, is similar to Fig. 3. Due to the limited resolution of most imaging systems, integer pixel locations found with this coarse search is not sufficient and sub-pixel level matching is required to get accuracies in micro-strain range. Some type of image interpolation is needed to achieve this objective. Figure 4 shows the interpolation schemes which are normally used. In this work, cubic spline interpolation was used due to the uniform transitions from pixel to pixel gray values achieved with this interpolation scheme.

Once the algorithm reaches in the vicinity of target point, the sub-pixel accurate location of target point is calculated by initiating a fine search. The fine search algorithm uses the response surface of the correlation coefficient in the neighborhood of target point to estimate its exact location with sub-pixel accuracy [14].

IV. EXPERIMENTAL SETUP

The experimental setup is similar to the one given in [14] and consisted of a high resolution Nikon D90 digital camera which records video streams at HD resolution (1280 X 720 pixels) and Sony XR-550 high definition camcorder which records video streams at full HD resolution (1920 X 1080 pixels). Use of two cameras for strain measurement is not essential but was done only to compare sensitivity of strain measurements from different imaging sensors.

Specimen surfaces were spray painted full black (or white) to form a uniform background. After the base color dried, a fine mist of white (or black) was sprayed to form a random speckle pattern as shown in Fig. 5. One camera was placed in front of each of the two faces of the specimen and the distance was adjusted between the camera and the specimen to properly frame the area of interest. For enhancing the contrast, specimens surface were illuminated by flexible fiber optic dual halogen lamps (Meiji Techno, Japan). By properly adjusting the orientation and distance of the two white light sources, a relatively uniform light intensity was generated on the specimen. The experimental setup with a Sony camcorder is shown in Fig. 6.

The materials selected for this study were aluminum alloy 2024-T6, E-glass/polyester laminate and epoxy impregnated specimens of carbon fiber tows. Tensile properties of the materials used in this study are listed in Table 1. Rectangular metallic strips were cut from the longitudinal direction of the sheets and dog-bone shape tensile specimens were machined.

The dimensions of the metallic samples were in conformance with ASTM standard E8-99.

Carbon fiber tow specimens were fabricated from 12k carbon fiber tow (T700S, Torayca, Japan), resin (epoxy) impregnated and cured in an autoclave at 150°C for 6 h under vacuum. Special care was given to avoid formation of resin lumps, uneven cross-section or filament breakage during specimen fabrication. Especially designed end tabs were cast on resin-impregnated tows to prevent slippage or failure within the grips and to facilitate proper transferring of load (Fig. 7). In majority of specimens the volume percentage of fiber and resin was kept approx. 60:40. Dimensions were set in accordance with ASTM standard D 4018-99 [16].

E-Glass/polyester laminates were prepared by impregnating the 2 stacked plies of E-glass woven fabric (type: plain weave, 0° / 90° direction, specific mass: 600 gm⁻²) in unsaturated polyester thermoset resin using vacuum assisted resin transfer molding (VARTM) process and cured at room temperature. Thickness of the samples was about 1.0 mm and other dimensions were set in accordance to ASTM standard D 3039-99 [19]. Picture of E-glass/polyester laminate specimen is shown in Fig. 8.

All the tension tests were performed on 150 kN servo-electric universal tensile testing machine (Tinius Olsen, UK) under crosshead speed of about 20 mm/min at room temperature. Axial alignment of the specimens in the wedge action grips was done with the help of LCD grid. At least three specimens of each material were tested.

For validation of measured axial strains electric resistance-type strain gages (Vishay Micro Measurements, USA) of about 6.35 mm gage length and 350Ω were used. Strain gage data was acquired by custom-made LabView 2010 software interface using National Instrument Data Acquisition System.

V. EXPERIMENTS AND RESULTS

During the tensile tests, images of the specimen surfaces were acquired at constant time intervals. These images were stored in AVI format which were imported and processed with our indigenously developed Optical Strain Measurement (OSM) utility in MatLab® environment. Instead of doing a full field strain measurement – as is normally done in commercial DIC software – only two markers were placed in the axial direction for displacement read out. The displacement data was then converted to engineering strain in post processing.

The inherent noise in the DIC results, which stems from the noise in imaging sensor output, was removed with a Gaussian filter of 10 pixel length and a standard deviation of 2. Further averaging of consecutive frames was done to reduce the effects of small vibrations and light intensity variations.

Fig. 9 shows the elastic part of Stress-Strain curve for an AA 2024-T6 specimen. Due to initial preload and toe effect, the curve does not pass through the origin; accordingly the fitted line was not constraint to pass through origin. The slope of fitted solid line defines the Young's modulus which is given in Table II.

Fig. 10 shows the Stress-Strain curve for a carbon fiber tow.

The corresponding tensile chord modulus was calculated as per ASTM standard D 4018-99 for a strain range of 0.1% to 0.6%. Fig. 11 shows the Stress-Strain curve for E-glass/polyester laminate. The tensile chord modulus was computed by a similar technique as per ASTM standard D3039-99. The initial part of the curve was excluded from the chord modulus range to remove the effect of initial bending of specimen. The average modulus along with observed standard deviations for carbon fiber tows and E-glass/polyester laminates are also given in Table II.

As shown in Table II, the measured values of Young's modulus for the materials under study are very close to literature data whereas the standard deviation in DIC results is on a higher side. This relatively high standard deviation, although still within acceptable limits, could be due to number of reasons. One possible reason is the low image quality because the digital cameras used for this test were not scientific grade and hence show more noise which could not be completely removed by Gauss filter. Another possible reason for this deviation is specimen alignment and bending which were only ensured visually. A very small misalignment between the image plane and specimen surface can result in significant false strains due to the out of plane motion.

VI. CONCLUSION

Application of Digital Image Correlation technique has been successfully demonstrated for measurement of Young's modulus of metallic as well as composite materials. For aluminum alloy, which exhibits an approximately same elastic range as the specified strain range for chord modulus measurement in carbon fiber tow, the modulus values obtained with this technique are in good agreement with strain gage data. The modulus of carbon fiber tows was only calculated with DIC and is very close to the supplier specifications.

Especially for carbon fiber tow, use of such a non-contact strain measurement technique allows accurate measurement of elastic constant without interfering with the loading condition. A contact type extensometer, for example, would cause significant bending of the carbon fiber tows and may result in premature failure. The narrow specimen width also excludes the possibility of mounting strain gages on the specimen, further highlighting the need for a non-contact strain measurement technique. Another benefit of using DIC for strain measurement is the cost reduction due to avoiding expensive gages. With Digital Image Correlation, it is possible to take measurements at different locations within the gage section. This makes it possible to check if there is non-uniform deformation within the specimen.

ACKNOWLEDGMENT

We wish to thank Dr. Sajid Mirza (Senior Chief Manager) for their valuable suggestions and guidance and Mr. Ahmed Bilal (Chairman SUPARCO) for approval and provision of facilities. We would further like to acknowledge the technical assistance and meaningful discussion extended by Mr. Tasleem Baig (Chief Manager) and Dr. Rasheed Ahmed

Baloch (Deputy Chief Manager) throughout the experimental work.

REFERENCES

[1] N. Parveen and G. V. S. Murthy, "Determination of elastic modulus in nickel alloy from ultrasonic measurements", *Bull. Mater. Sci.*, vol. 34, no. 2, pp. 323-326, April 2011

[2] D. Ensminger, *Ultrasonics – Fundamental, Technology, Applications*, New York: 2nd ed, Marcel Dekker Inc., 1988 [3] P. McIntire, Ed., *Nondestructive Testing Handbook: Ultrasonic Testing*, American Society for Nondestructive Testing, USA, 2nd ed., vol. 7, 1991

[4] Q. M. Wang and L. Eric Cross, "Determination of Young's modulus of the reduced layer of a piezoelectric RAINBOW actuator", *J. Appl. Phys.*, vol. 83, no.10, pp. 5358-5363, 1998

[5] L. Kiesewetter, J.M. Zhang, D. Houdeau and A. Steckenborn, "Determination of Young's Moduli of micromechanical thin films using the resonance method", *Sens. Actuat. A-Phys.*, vol. 35, no. 2, pp. 153-159, Dec. 1992

[6] J. Gubicza, "Determination of Young's Modulus from depth sensing Vickers Indentation Tests", *Solid. State Phenom.*, vol. 56, pp. 195-200, 1997

[7] S. Hong, T. P. Weihs, J. C. Brayman and W. D. Nix, "Measuring stiffnesses and residual stresses of silicon nitride films", *J. Electron. Mater.*, vol. 19, no. 9, pp. 903-909, 1990

[8] G.M. Pharr, W.C. Oliver, and F.R. Brotzen, "On the generality of the relationship among contact stiffness, contact area, and elastic modulus during indentation", *J. Mater. Res.* vol. 7, pp. 613-617, March 1992

[9] J. B. Pethica, R. Hutchings, and W. C. Oliver, "Hardness measurements at penetration depths as small as 20 nm", *Philos. Mag. A*, vol. 48, no. 4, pp. 593-606, 1983

[10] K. M. Mussert, W. P. Vellinga, A. Bakker and S. Van der Zwaag, "A nano-indentation study on the mechanical behaviour of the matrix material in an AA6061 – Al₂O₃ MMC", *J. Mater. Sci.*, vol. 37, pp. 789-794, 2002

[11] T. Rio, Go'mez-Del, P. Poza and J. Rodri'guez, "Micromechanical characterization of Al 8090/SiC composites by nanoindentation", *J. Mater. Sci.*, vol. 40, no. 6, pp. 1513-1515, 2005

[12] T. Kwaaitaal and A. J. G. Schoofs, "Determination of Young's Modulus or Poisson's Ratio Using Eddy Currents", *Exp. Mech.*, vol. 19, no. 12, pp. 450-455, March 1979

[13] K. E. Fällström and M. Jonsson, "A nondestructive method to determine material properties in anisotropic plates", *Polym. Compos.*, vol. 12, no. 5, pp. 293-305, Oct. 1991

[14] M. Z. Siddiqui, F. Tariq and N. Naz, "Application of a two step digital image correlation algorithm in determining Poisson's ratio of metals and composites", presented at Materials and Structures Symposium, 62nd International Aeronautical Congress, South Africa, Oct. 2-5, 2011.

[15] ASM Aerospace Specification Metals Inc. Available: <http://asm.matweb.com/search/SpecificMaterial.asp?bassnum=MA2024t6>

[16] *Standard Test Methods for Properties of Continuous Filament Carbon and Graphite Fiber Tows*, ASTM Standard D 4018, 1999

[17] Torayca T700S Data sheet, Technical data sheet no. CFA-005, America

[18] *Mechanical Properties of Carbon Fibre Composite Materials*, Available: <http://www.performance-composites.com>

[19] *Standard Test method for Tensile Properties of Polymer Matrix Composite Materials*, ASTM Standard D 3039, 1999

| | | | |
|----------------------------|------|-----|-----------|
| Elongation at fracture (%) | 9-10 | 1.8 | 1.75 |
| Poisson's ratio | 0.33 | - | 0.20-0.22 |

^a This value depends upon fiber/resin volume percentage and principal loading direction.

^b This value is for 60% fiber volume percentage. The value of vL depends upon fiber/resin volume percentage and principal loading direction.

TABLE II
MODULUS OF ELASTICITY (IN GPa)

| Material | Literature | Strain gages | DIC |
|----------------------------|------------|--------------|----------|
| AA 2024-T6 | 72.5 | 73.4±0.6 | 73.5±2.5 |
| Carbon Fiber Tow* | 230 | - | 228±8 |
| E-Glass fabric composite** | 22-25 | 22.4±2 | 23.9±2 |

All units are in GPa.
* strain range: 1000-6000 µε
** strain range: 2300-6000 µε

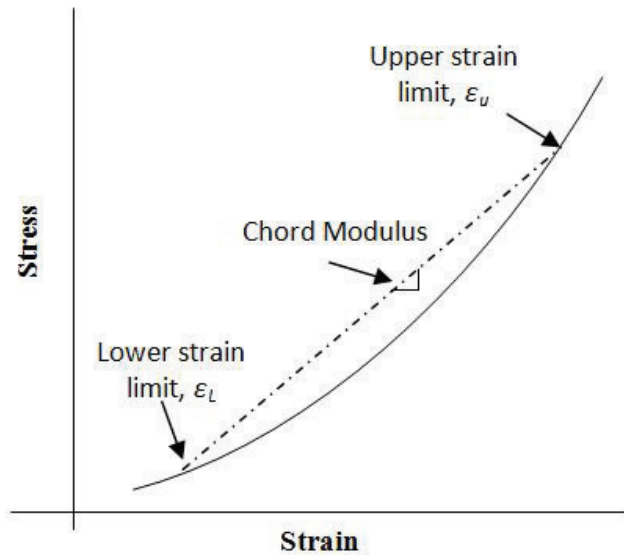


Fig. 1. The slope of dotted line is the chord modulus as defined in ASTM standard D4018-99 [16]

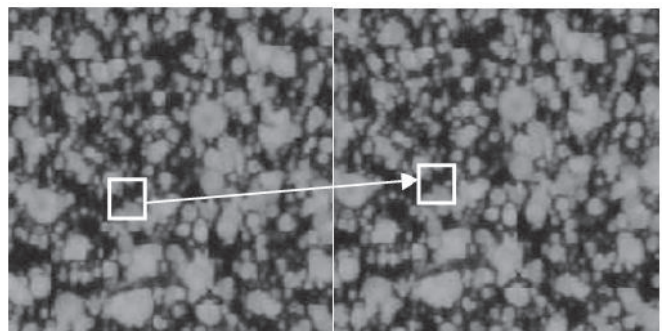


Fig. 2. Displacement of an image point after application of load

TABLE I
TENSILE PROPERTIES OF MATERIALS USED IN THIS WORK

| Property | AA 2024-T6 [16] | Carbon Fiber Tow [17] | E-Glass/Polyester Laminate [18] |
|----------------------------------|-----------------|-----------------------|---------------------------------|
| Young's Modulus (GPa) | 72.5 | 230 | 22-25 |
| 0.2% offset Yield Strength (MPa) | >345 | - | -- |
| Ultimate tensile strength (MPa) | >427 | 4900 | 440 |

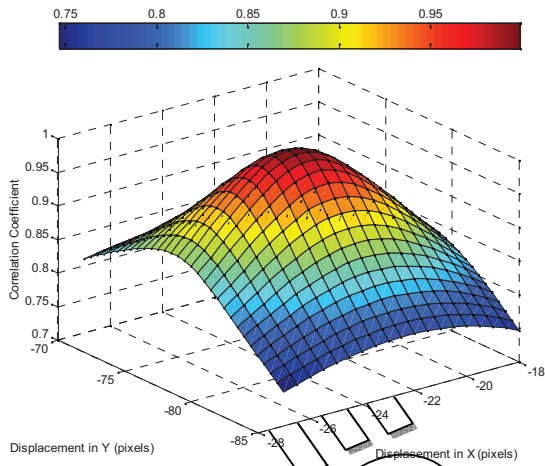


Fig. 3. Correlation coefficient as a function of X and Y displacements

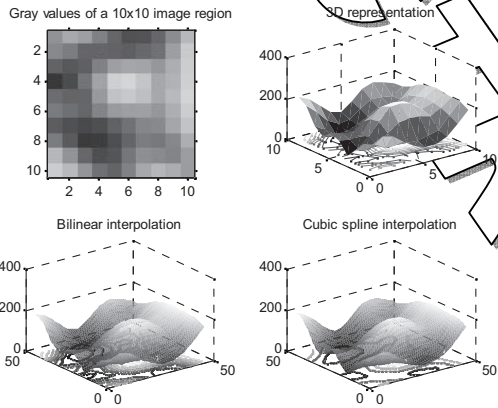


Fig. 4. Three dimensional representation of gray values in original and interpolated images for different interpolation schemes



Fig. 5. Two types of speckle patterns with white and black background are shown. As long as the speckle size remains the same, the choice of background color does not affect the correlation



Fig. 2. Experimental setup for uniaxial tensile tests. The digital camera is positioned in such a way that the area of interest remains in the frame. Halogen lamps are visible in the foreground illuminating the specimen surface with controlled light intensity suitable for correlation.



Fig. 7. Epoxy impregnated specimens of unidirectional carbon fiber tows

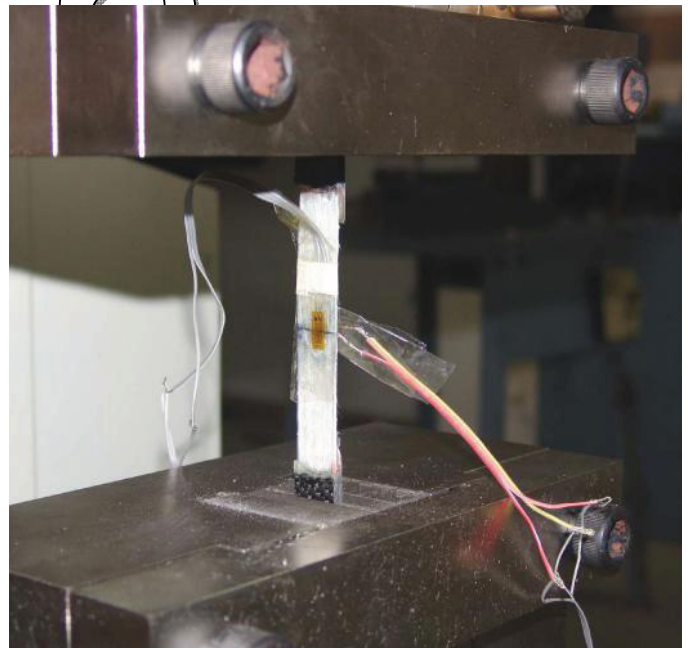


Fig. 8. E-glass/polyester laminate specimen with strain gage mounted for measurement of elastic modulus

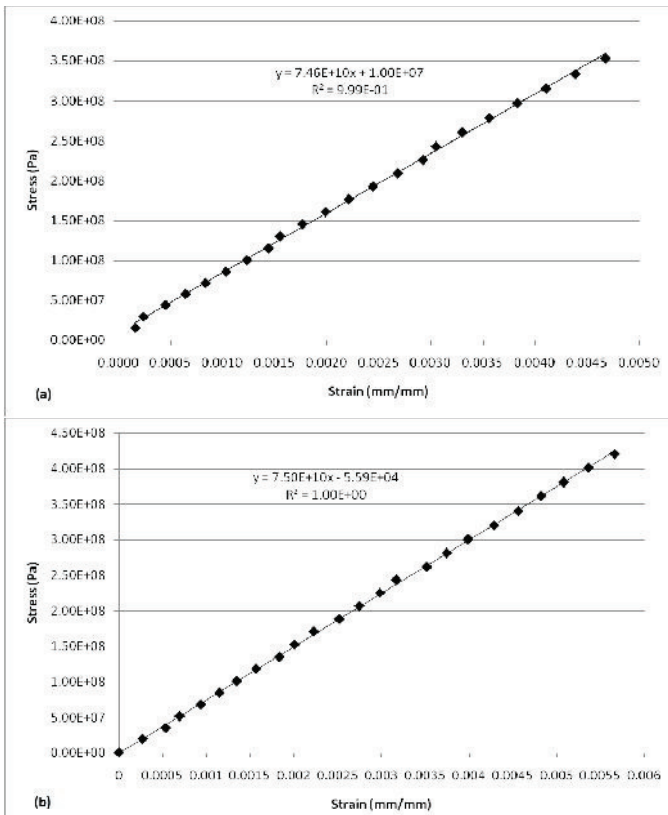


Fig. 3. Stress-strain curve for an Aluminum alloy 2024-T6 specimen in the elastic region with strain measurement done through (a) strain gauge and (b) DIC

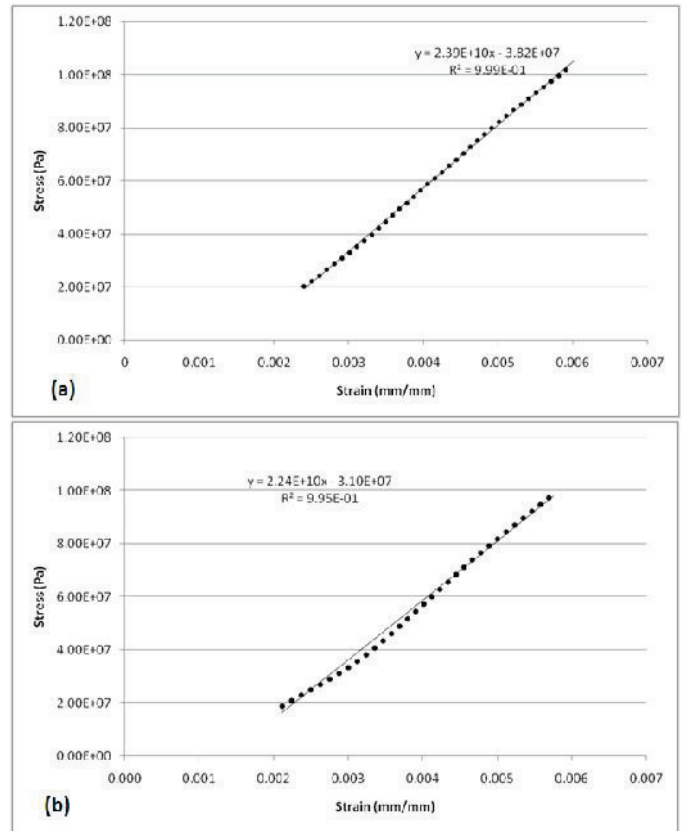


Fig. 5 Stress-strain curve for an E-glass/polyester laminate specimen in the strain range for chord modulus with strain measurement done by (a) DIC and (b) strain gauge

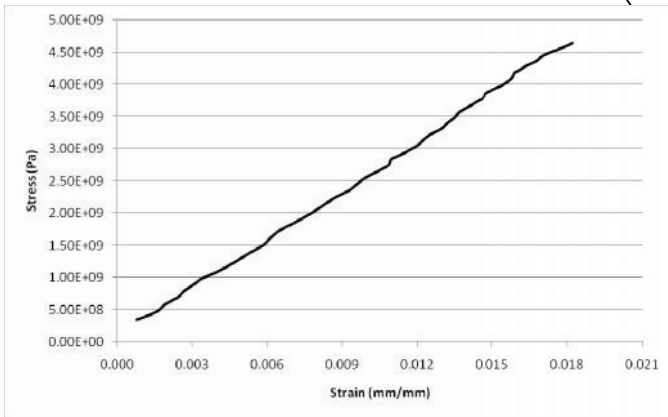


Fig. 4. Stress strain curve for a Carbon fiber tow. Note the essentially linear behavior up to failure. The strain range for chord modulus as per ASTM standard D4018 is 0.1% to 0.6%.